RELATIONSHIP BETWEEN ELECTRIC CURRENTS, PHOTOSPHERIC MOTIONS, CHROMOSPHERIC ACTIVITY, AND MAGNETIC FIELD TOPOLOGY

L. VAN DRIEL-GESZTELYI
Astronomical Institute, University of Utrecht, 3508 TA Utrecht, The Netherlands
and
Kiso Observatory, Institute of Astronomy, University of Tokyo, Mitake-mura, Kiso-gun, Nagano-ken, 397-01 Japan

A. HOFMANN
Astrophysikaliches Institut Potsdam, Sonnenobservatorium Einsteinturm, D.O.-1561 Potsdam, Telegrafenberg, Germany

P. DÉMOULIN, B. SCHMIEDER
Observatoire de Paris, DASOP, URA 326, CNRS, 92195 Meudon Cédex, France

and

G. CSEPURA
Heliophysical Observatory of the Hungarian Academy of Sciences, H-4010 Debrecen, Hungary

(Received 28 October, 1992; in final form 7 July, 1993)

Abstract. Through coordinated observations made during the Max'91 campaign in June 1989 in Potsdam (magnetograms), Debrecen (white light and Hα), and Meudon (MSDP), we follow the evolution of the sunspot group in active region NOAA 5555 for 6 days. The topology of the coronal magnetic field is investigated by using a method based on the concept of separatrices – applied previously (Mandrini *et al.*, 1991) to a magnetic region slightly distorted by field-aligned currents. The present active region differs by having significant magnetic shear. We find that the Hα flare kernels and the main photospheric electric current cells are located close to the intersection of the separatrices with the chromosphere, in a linear force-free field configuration adapted to the observed shear. Sunspot motions, strong currents, isolated polarities, or intersecting separatrices are not in themselves sufficient to produce a flare. A combination of them all is required. This supports the idea that flares are due to magnetic reconnection, when flux tubes with field-aligned currents move towards the separatrix locations.

1. Introduction

In the highly conductive solar atmosphere the magnetic field is believed to be stressed at the photospheric level by convective motions. They induce field aligned currents in the tenuous corona above, which are stored there as free magnetic energy which can be released rapidly while keeping the photospheric boundary unchanged. When strong enough electric currents are present in the corona, they can cause an ideal instability of the whole magnetic configuration, leading to release of stored energy in form of flares or surges (see, e.g., Somov, 1986; Démoulin, Priest, and Ferreira, 1991; Abramenko, Gopasyuk, and Ogir, 1991). It is possible to infer current densities from photospheric vector magnetic field measurements. Current densities indicate places where large-scale flux bundles leave or enter

Solar Physics **149:** 309–330, 1994.

the photosphere with a non-potential character, i.e., places with stored magnetic energy.

In this paper we attempt to identify locations of stored energy in a solar active region which delimit the current cells in the photosphere. The white-light, Hα, and magnetic observations used are described in Section 2. We compare the proper motion of sunspots (Section 3), which represent the footpoints of the magnetic loops in the active region, with the development of strong photospheric currents in space and time (Section 4).

Abramenko, Gopasyuk, and Ogir (1991) found that flare kernels tend to appear in places where strong electric current is flowing upward, from the photosphere towards the chromosphere. This result is surprising, since it suggests some morphological difference should exist between flare activity in the two hemispheres, where the magnetic polarities, and therefore the direction of the currents, are reversed. In the present paper we analyse the locations of strong photospheric currents and different kinds of chromospheric activity in order to find out if they are related to each other (Section 5).

Recent development in MHD theory shows that magnetic release of energy takes place on singular surfaces (called separatrices), which separate magnetic fluxes of different connectivities (see, e.g., Priest, 1991, and references therein). Because of the frozen-in condition, current sheets are naturally created on the separatrix surfaces, when a magnetic configuration is deformed, e.g., as a result of photospheric motions (see Vekstein, Priest, and Amari, 1991, and references therein). On these surfaces finite resistivity must be taken into account and reconnection should occur. A favourable site for energy release is at the intersection of separatrices (namely at the separator), where magnetic field lines of four velocity regions can exchange their photospheric link in a dynamical process.

Various flare observations suggest the qualitative picture that solar flares are caused by interaction of large-scale structures and that the process of energy release cannot be considered separately of the evolution of the entire active region (Schmieder *et al.*, 1991; Gaizauskas, 1989). Some attempts have been made to apply these ideas to observations by calculating the positions of the separatrices in the extrapolated potential field (Gorbachev and Somov, 1988; Mandrini *et al.*, 1991, 1993, Démoulin *et al.*, 1993). The positions of the flare kernels and of the current concentrations have been found close to the intersection of the separatrices with the photosphere. It is interesting to go further by analysing an active region which has a significant amount of shear. A summary of the present results is presented in Section 7.

2. Observations

2.1. WHITE-LIGHT AND Hα OBSERVATIONS IN DEBRECEN

Several series of white-light full disk photoheliograms and Hα frames obtained at Heliophysical Observatory of the Hungarian Academy of Sciences in Debrecen

TABLE I
Observations of the AR 5555

Date 1989	White-light	MSDP Hα	Magnetograph B	Flares (Hα) Meudon/Debrecen	X-ray
22 June	13:16–13:51				
23 June	06:44–06:51	15:11–15:55	11:58–13:02	12:49 (SN)	
			13:37–14:05	13:30 (SN)	
				14:21 (SN)	
				15:06 (SF)	
24 June	12:57–13:03	06:52–07:53		07:48 (SF)	
		08:22–08:46			
		08:50–09:30			
		13:02–15:03		13:46 (SF)	C 4.1
		15:41–15:25		15:38 (SF)	C 7.6
25 June	07:51–07:57	06:40	06:15–07:10	07:20 (SF)	
		06:48–12:07	09:02–09:55	09:43 (SF)	C 1.8
		12:10–17:17		16:31	
26 June	07:50–08:37	08:15–14:51	05:20	08:50 (SN)	
			07:07		
			08:30	13:29 (surge)	
27 June	07:26–07:32				

and its Gyula Observing Station are used for a study of the motion and evolution of the sunspot group in the period of 22–27 June, 1989. The observations are listed in Table I. The positions of the sunspots are determined from the full-disk heliograms by procedures described in detail by Dezsö, Gerlei, and Kovács (1988).

Hα filtergrams are obtained in Debrecen with a 53-cm Nikolsky-type coronagraph, equipped with a 0.5 Å Halle filter. The diameter of the solar disc at the Coudé focus is 12.5 cm. A portion of this disc is photographed on 35-mm Kodak Solar Patrol film. The observational procedure consists of taking Hα ± 1 Å, Hα ± 0.5 Å, and Hα sequences of frames.

2.2. Vector Magnetic Field Observations in Potsdam

The photospheric vector magnetic field of active regions is measured by a step-modulated vector magnetograph of the Einsteinturm Solar Observatory at Potsdam in the wings of the line Fe I 5250.20 Å. A total polariser and a $\lambda/4$ plate in front of the first coelostat mirror are used to calibrate the instrument before and after each scan. During the measurement an inclined glass plate compensates for the main contribution of linear polarization caused by the telescope itself. The Stokes vectors measured during the scanning of the active region are corrected by taking into account the time variation of the instrumental calibration matrix as well

as influences of stray light. The corrected Stokes vectors (i.e., polarizations) are transformed into magnetic vectors by means of Staude's (1970a, b) calibrational functions, using different model atmospheres for umbrae and for the photosphere, and taking into account the true slit dimensions and the Faraday effect. The r.m.s. noise level corresponds to about 10 G for the longitudinal, and to 100 G for the transverse fields.

2.3. Hα OBSERVATIONS IN MEUDON – SPECTROHELIOGRAPH AND MSDP

The Multi-channel Subtractive Double Pass spectrograph (MSDP) operates on the Solar Tower at Meudon (Mein, 1977). The MSDP records an $8' \times 1'$ area of the solar surface with spatial and temporal resolutions of $\sim 2''$ and 10 s, respectively. Observations of the same region are obtained simultaneously at 9 wavelengths in the Hα line, from which a two-dimensional set of profiles is reconstructed. Maps of the intensity fluctuations and Doppler-shifts are derived using a standard method (Mein, 1977). A larger field of view ($5' \times 8'$) is obtained by adding five elementary fields taken within 60 s.

The intervals of Hα (MSDP) observations in Meudon, the magnetograph observations in Potsdam, and the list of flares observed at Meudon and Debrecen are given in Table I.

3. Proper Motion of Sunspots in the Active Region

AR NOAA 5555 was first observed on 20 June, 1989 (N25, E77, *Solar Geophysical Data*) as a small active region. One day before it was just at the east limb, and one rotation earlier two small active regions were present at the same location. On 21 June, AR 5555 was a developed bipolar sunspot group. On 22 June it appears (see Figure 1) as a bipolar region in a developed stage with a big preceding spot (*S1*) and smaller following spots. The entire region is situated at a high latitude between 24.5° and 29°, where the effect of differential rotation is quite strong. The mean rotation velocity of the sunspots is considerably lower than the Carrington rate and there is even a strong shear between the low and the high latitude boundaries of the active region, as shown in Figure 2.

The proper motions observed in a sunspot group usually characterize the stage of development of the group. Between 22 and 23 June the principal preceding spot *S1* still moves faster than the mean differential rotation speed at this latitude (Newton and Nunn, 1951), which indicates that the sunspot group is probably not older than 3–5 days, only formed behind the eastern limb and therefore the initial divergence of its principal spots is not over yet (in Figure 2 we compare the daily displacement of spots to the expected displacement caused by differential rotation). Between 23 and 26 June this divergence stops and spot *S1* starts to move with the differential rotation speed at this latitude, while between 26 and 27 June it moves even slower than that. The motions clearly show that after 26 June the sunspot group passes its stage of maximum development and starts disintegrating. This can

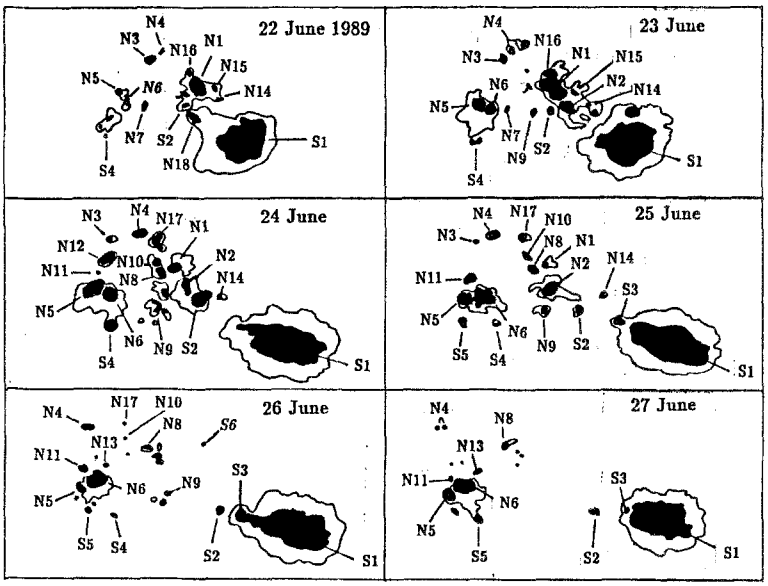

Fig. 1. Drawings based on white-light observations (Debrecen) of AR 5555 between 22 and 27 June, 1989. Note that the drawings are neither corrected for perspective effects due to the position of the AR on the solar disc, nor are they centered on the same Carrington coordinates. North and south magnetic polarities are labeled by N and S, respectively. In all figures north is up, east is left.

also be seen comparing the panels of 25 and 27 June in Figure 1.

Based on the evolution pattern (Figure 1), the relative proper motions (Figure 2), and photospheric magnetic fields (Figures 3 and 4) we simplify the description of the region by associating the spots in groups (see Table II). Besides the main bipole formed by *S1*, *N1*, *N2*, *N3*, *N4*, and other small spots $(1,\ 2+2')$ there are three other bipoles: *S2*, *N14* (3, 4), *S4*, *S5*, *N5*, *N6*, *N11* (5, 6), and from 25 June *S3*, *N9* (7, 8). The orientation of the bipole (7, 8) is parallel to the main bipole, while (5, 6) is almost perpendicular to it. The orientation of (3, 4) is the most peculiar: it is reversed, disobeying Hale's law. Moreover, the strongest shear of sunspot motions in the AR appears between bipoles $(1,\ 2+2')$ and (3, 4) (Figure 2); thus they play a very important role in the activity of the region.

4. Current Analysis in the Active Region

4.1. Analysis of Magnetograms

The observed region is relatively far from the disk center (N29°, E50°, and E26° on 23 and 25 June, respectively), and therefore the longitudinal component of the magnetic fields has a non-negligible contribution coming from the horizontal field component, which introduces false polarities in the longitudinal map with intensities up to 100 G. From the position of the active region on the solar disc and a presumed degree of divergence of field lines above spots, we deduce qualitatively

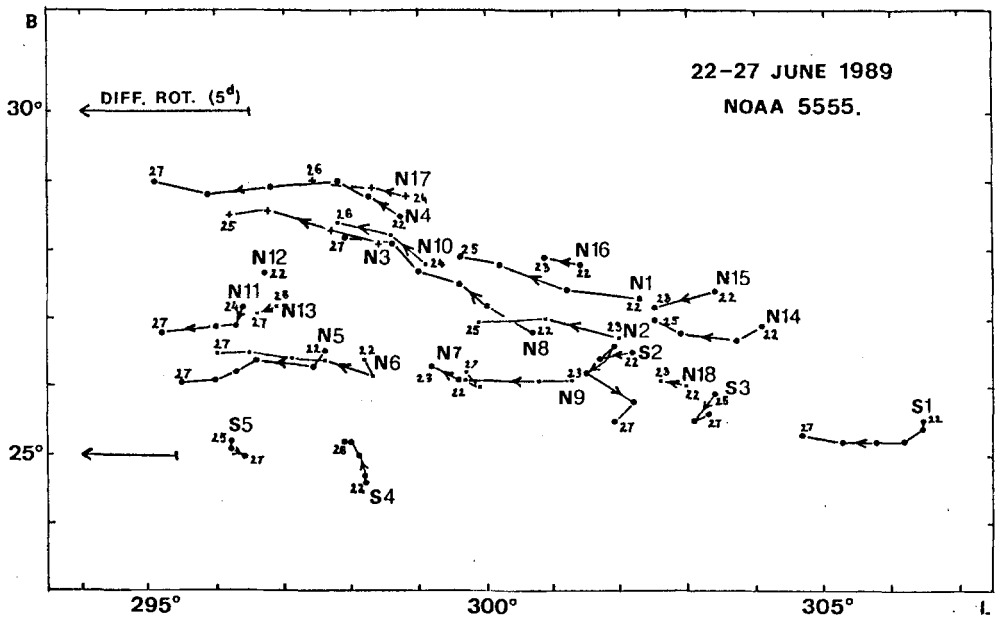

Fig. 2. Proper motions of sunspots in AR 5555 in Carrington coordinates between 22 and 27 June, 1989. Small numbers indicate days of the month. Note that the Carrington network rotates rigidly, while sunspots rotate differentially, which causes an apparent eastward motion of these high-latitude spots in the Carrington coordinates. Arrows in the upper and lower left corners of the panel indicate the displacement caused by differential rotation at 30° and 25° latitude, respectively, during a 5-day period, following Newton and Nunn (1951). For denotations of spots see Figure 1.

TABLE II

Definition of the spot groups used in the separatrix computations

Group	23 June	25 June
1	*S1*	*S1*
2	*N3, N4, N7, N8, N9*	*N3, N4, N8, N10, N17*
2′	*N1, N2, N15, N16*	*N1, N2*
3	*S2*	*S2*
4	*N14*	*N14*
5	*S4*	*S4, S5*
6	*N5, N6*	*N5, N6, N11*
7		*S3*
8		*N9*

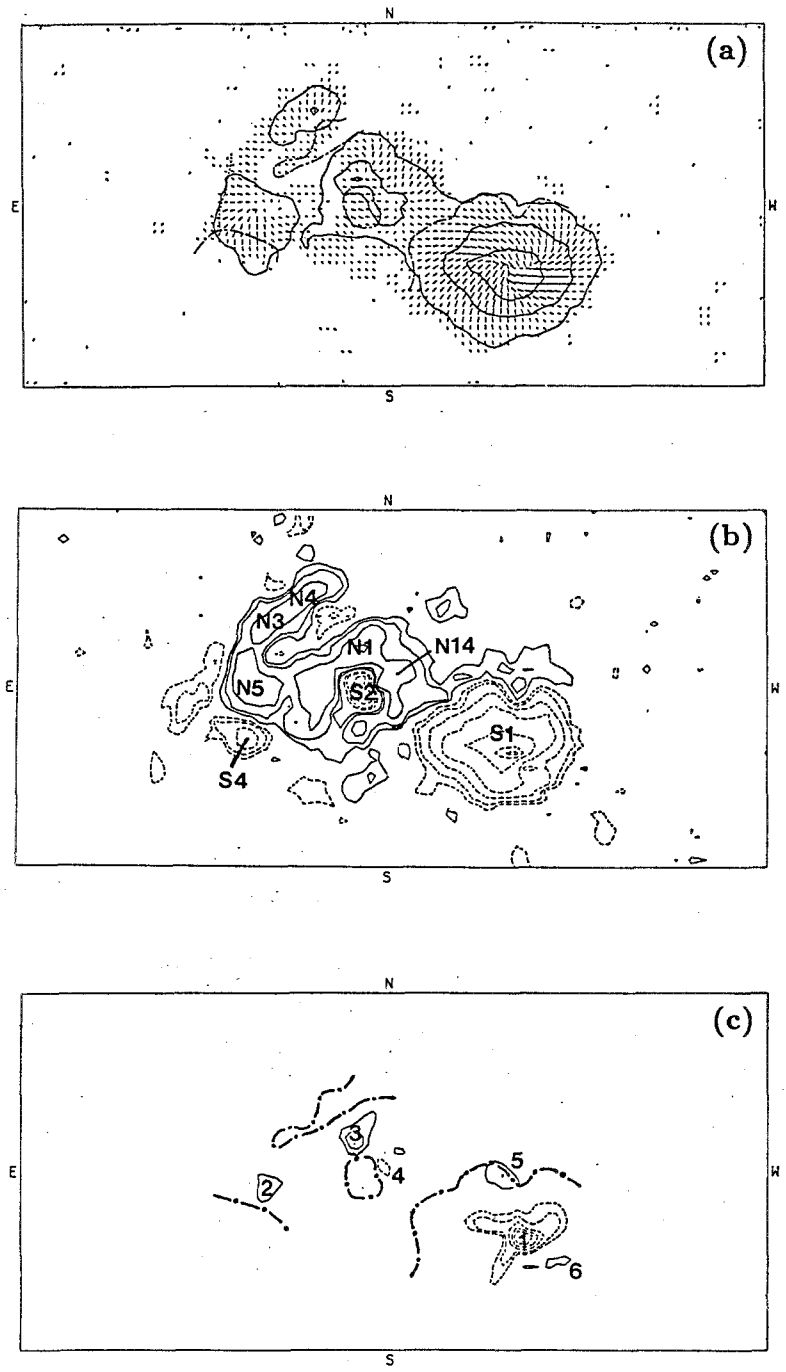

Fig. 3. Potsdam magnetic map on 23 June, 1989 transformed to local solar coordinates: (a) white-light spot contours with horizontal magnetic field direction (the three lengths of the segment represent the field strength B_h = 300, 600, 900 G), (b) vertical magnetic field contours (isocontours level are for $B_z = \pm 40$, 80, 160, 320, 640, 960, 1280 G), (c) vertical current density (isocontours level are for $J_z = \pm 0.3$, 0.5, 0.7, 1, 1.2 $\times$ 10^{-2} A m^{-2}, the lowest isocontour being the first significant level). The dotted-hatched lines show the neutral lines statistically of the observed vertical field, B_z.

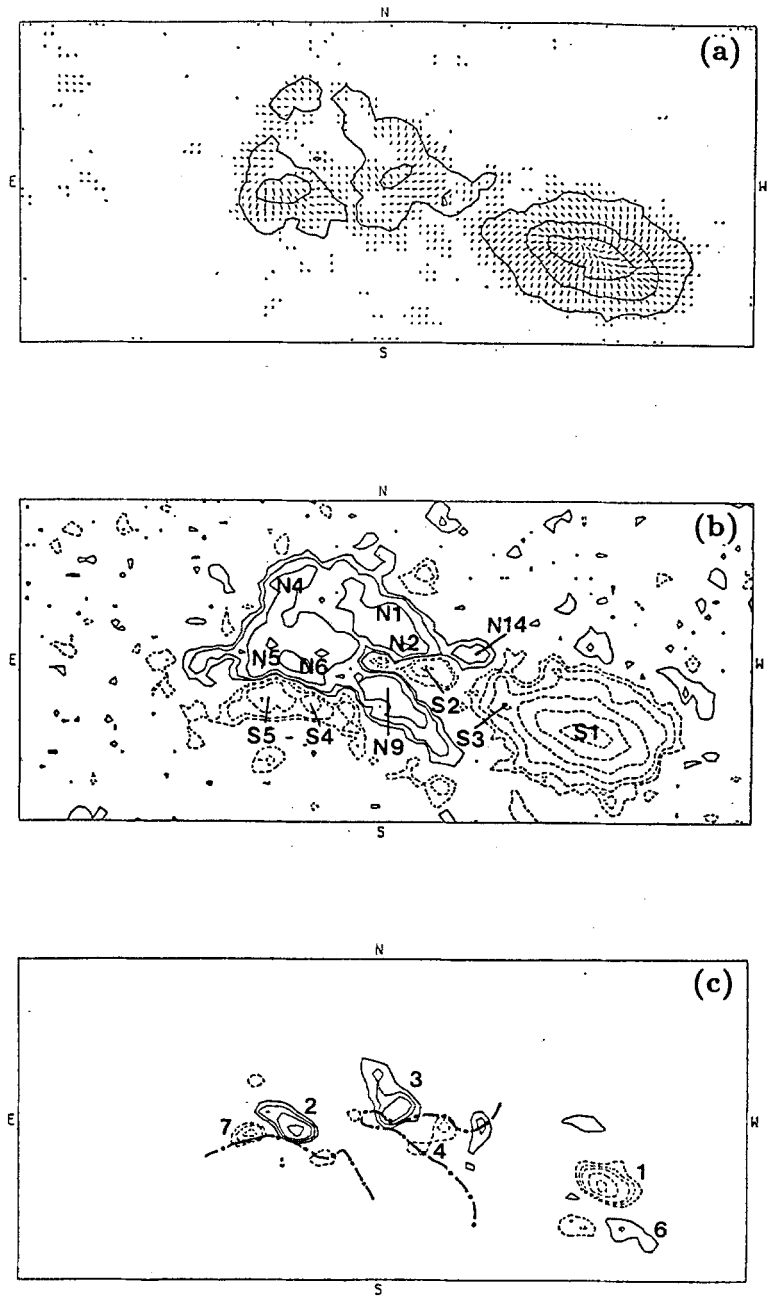

Fig. 4. Same as Figure 3 for the magnetic field on 25 June, 1989.

that these false polarities are located to the north and the east of the strong field concentrations. After removing the sign ambiguity in the observed transverse field component, taking the closest solution to the potential field, we transform the observed field to the horizontal and vertical local solar coordinates (Figures 3 and 4). This transformation only partially removes the false polarities, because the noise level in the transverse field is of order 100 G. The false polarities can be recognized quantitatively by comparing the observed and transformed magnetograms: after transformation the field component decreases in them and only field intensities up to 50 G remain, which can be attributed to the noise in the transverse field. A confirmation can be made by comparing the magnetograms of several days at places where no sign of flux emergence is seen in Hα. From this analysis we deduce that the negative polarities to the east of N5, in between N3, N14, and N16, and the positive polarity to the north of S1 are false polarities. They are therefore discarded from the model (Section 6). In the same way, the current cells found in these regions are quite doubtful (Section 4.3).

4.2. Computation of current density

The method of inferring current densities from photospheric vector magnetic field measurements are described in earlier papers (see, e.g., Hofmann, Ruždjak, and Vršnak, 1989; Hofmann and Kálmán, 1991). The calculation and handling of currents are still quite problematic, so there are relatively few attempts to carry out such analysis (see Hagyard, 1988; Canfield, de La Beaujardière, and Leka, 1991; Wilkinson, Emslie, and Gary, 1992, and references therein).

To infer current densities from photospheric vector magnetic field data one has to calculate derivatives, meaning that only large-scale currents, which are extended over an area of more than two pixels in both directions, can be derived. Therefore the small-scale currents, which can also play an important role in the activity of the region, cannot be traced. Taking derivatives increases the noise in the already noisy transverse field, and $B_\perp$ is reliable only if it is larger than $\approx$100 G. Therefore only currents flowing in strong magnetic fields can be obtained and currents loops connecting places of strong and weak magnetic fields (e.g., from a sunspot region to a facular region) appear unbalanced in the current density maps.

In the understanding of the current maps, the Hα fibrils and the computed field lines are of great help to find which currents are connected. The derived current density and the total net current detected are given in Tables III and IV, respectively. The errors given in the tables include the noise in the measurements and are calculated following Hagyard (1988).

The majority of the inferred current cells (cf. Figures 3(c) and 4(c)) can be identified and followed for several days, which shows their relative stability and reliability. Their development also follows the same pattern of evolution deduced from spot and magnetic field observations. But we also have to keep the systematic errors in mind: since the global magnetic configuration is nearly the same from day to day, the same systematic errors can persist. Thus, we base our conclusions

TABLE III
Current densities in AR 5555 in 10^{-2} in A m^{-2}

Date	Denotation of current cells						
June 1989	1	2	3	4	5	6	7
23	-30.7 ± 12.2	6.5 ± 5.8	7.6 ± 5.8	(-5.3 ± 5.8)	4.4 ± 3.8	2.7 ± 0.8	
25	-18.8 ± 6.0	11.6 ± 6.5	12.7 ± 9.1	-3.5 ± 3.0	2.1 ± 1.6	2.1 ± 0.9	-4.4 ± 3.0
26	-11.2 ± 4.8	12.9 ± 7.1	4.2 ± 3.0	(-1.0 ± 1.2)	2.1 ± 1.3	2.9 ± 1.3	-4.7 ± 3.3
27	-9.1 ± 4.4	4.7 ± 3.2	(1.0 ± 1.2)	(-1.6 ± 1.8)	(1.1 ± 1.2)	3.2 ± 1.6	-4.5 ± 3.5

TABLE IV
Net currents in AR 5555 in 10^{11} A

Date	Denotation of current cells						
June 1989	1	2	3	4 ?	5 ?	6 ?	7
23	-12.3 ± 4.9	2.6 ± 2.3	3.0 ± 2.3	(-2.1 ± 2.3)	1.8 ± 1.5	1.1 ± 0.3	
25	-7.5 ± 2.4	4.6 ± 2.6	5.1 ± 3.6	-1.4 ± 1.2	0.8 ± 0.6	0.8 ± 0.4	-2.0 ± 0.8
26	-4.5 ± 1.9	5.2 ± 2.8	1.7 ± 1.2	(-0.4 ± 0.5)	0.8 ± 0.4	1.2 ± 0.5	-1.9 ± 1.3
27	-3.6 ± 1.8	1.9 ± 1.3	(0.4 ± 0.5)	(-0.6 ± 0.8)	(0.4 ± 0.5)	1.3 ± 0.6	-1.8 ± 1.4

'?' indicates doubtful current cells.

mainly on the strongest cells (cells 1, 2, and 3), and the discussion of the other current cells in the following subsection needs to be regarded with some caution.

4.3. Observed currents

On 23 June (Figure 3) the main currents observed occur in the western part of the big leader spot *S1* (current cell 1) and in spot *N1* (current cell 3). In this system a current I_{31} flows from current cell 3 to the western part of current cell 1, parallel to the magnetic field lines. This loop system appears to extend quite high into the corona ($\approx$15 Mm), as suggested by the field-line computations (Figures 9(c) and 9(d)). A second system of currents I_{21} is found between the following-polarity spots *N5, N6* (current cell 2) to spot *S1* (south part of current cell 1). This current system does ot seem to influence the flare activity of 23 and 25 June (see Section 6). No other current cells can be related to current cell 1 of the leader spot.

We will now consider the current balance between the preceding and following polarities. The N polarity areas, where the currents I_{31} and I_{21} leave the photosphere, are situated in less concentrated field regions than the S polarity current

cell 1, and as a result of this $|I_2 + I_3| < |I_1|$ (cf. explanations in Section 4.2). Considering the different field strengths and concentrations in the current cells 1, 2, and 3, the currents I_{21} and I_{31} are both estimated to be about 5×10^{11} A.

Several authors (Lin and Gaizauskas, 1987; Ding *et al.*, 1987; Hagyard, 1988; Romanov and Tsap, 1990; Canfield, de La Beaujardière, and Leka, 1991) have found Hα flare kernels located close to, or at the position of current concentrations. Our results confirm these earlier works since we find that the current cells 1 and 3 are at the border of the flare kernels (see Figures 8(a), 8(b), 10(c), 10(d), and Section 5.2).

In the next few days current 1 weakens (Table IV) and the predominant twist of the transverse field observed on 23 June also becomes less pronounced (Figure 4(a)). The current cells 2, 3 do not follow this evolution: they grow respectively until 26 June and 25 June, then they decrease. On 25 June a new current (cell 7 in Figure 4(c)) appears in the vicinity of the current cell 2 together with new polarities.

The other current cells (4, 5, 6) are weak, and their existence is questionable. Current cell 4 is related to the spot *S2*, which belongs to the reversed bipole (3, 4). Current cell 5 is in a region where the projection effect is important (see Section 4.1), and it should therefore be discarded. Current cell 6 in the main leader spot has no counterpart in the following polarity (current cell 4 is the only candidate but it disappears on 26 June while current cell 6 remains) and we therefore discard it.

5. Filament and Flare Activity

5.1. Filament evolution

On 23 June we see two filaments around the sunspot group (Figures 6 and 7): one (*F1*) located to the north of the main following polarity, between spots *N5, N6*, and *S4* (close to current cell 2), runs mainly north–eastward; the other (*F2*) is located north of the leader spot *S1*. In both cases the filaments are at the periphery of the active region in low fieldstrength regions (where the magnetic field falls below our threshold of sensitivity). The eastern end of the filament *F1* remains connected to the group at the polarity inversion line between spots *S5* and *N5*. The new current cell 7 and the growing current cell 2 are possibly related to the filament activity (strong turbulent motions) observed in the region on 25 and 26 June. The filaments and the connecting filament channel expand around the sunspot group. In the period of 23 and 27 June they move away (to the north–east) from the sunspot group with decreasing speed (see Table V). As filaments are formed along the inversion line of the magnetic fields, the expanding motion of the filament channel is merely an indicator of the general expansion of the magnetic fields around the evolving active region.

TABLE V
Expansion velocities of the filaments around the sunspot group (in km s^{-1}). F1 and F2 are, respectively, the filaments located to the north–east and north of the active region.

Interval June 1989	F		F2
	Direction from the AR		
	Eastward	Northward	Westward
23–24	0.2	0.3	0.2
24–25	0.4	0.3	≈0
25–26	0.2	≈0	≈0
26–27	0.2	≈0	≈0

5.2. FLARE ACTIVITY IN THE ACTIVE REGION

According to *Solar Geophysical Data*, 5–16 flares occurred daily in the active region between 22 and 27 June for a total of 56; 4 flares gave rise to C or M class X-ray emission each day in the period of 22 and 25 June, and one on 26 and 27 June (see Table I). Eleven flares were observed in Hα at Meudon or Debrecen (see Figures 5 and 6). They occurred in the vicinity of spot *S2* (Figures 5 and 6) on 23 and 25 June, while on 26 June a flare was observed at a different site by Meudon.

On 23 June, small flares consisting of bright patches erupted around the spot *S2*, as well as in the northern part of the penumbra of the big leader spot *S1* (Figure 5).

On 24 June at 13:45 UT (Figure 6) chromospheric activity starts with the appearance of a flare close to the place of the spot *S2*, which is the center of flare activity all day. Taking into account only the brightest ribbons, it is a two-ribbon flare of peculiar shape: one ribbon is relatively straight running from the spot *S2* to the NE part of the penumbra of *S1*, while the other ribbon is almost circular around *S2* outlining this isolated S polarity island embedded in N polarity fields, leaving only a narrow opening for the other ribbon at the western side. Besides the main flare, ribbon-like brightenings appear at remote places such as both to the eastern end of *F1* and to the north–east of *S1*.

On 25 June the shape of the flare ribbons is less complicated, but still the same places in the sunspot group seem to play a role in the flare process (see Figure 5). On the other hand, the flare observed on 26 June at 08:52 UT is linked to the weak spots of *S6* and *N8*. Chromospheric brightenings can be seen on both sides of the inversion line in their vicinity. This fact shows that the magnetic configuration underwent a basic change by 26 June, since *S2* is no longer an isolated island of S polarity in a N polarity environment, but gets out into S polarity fields and ceases to function as the center of flare activity (Figure 6).

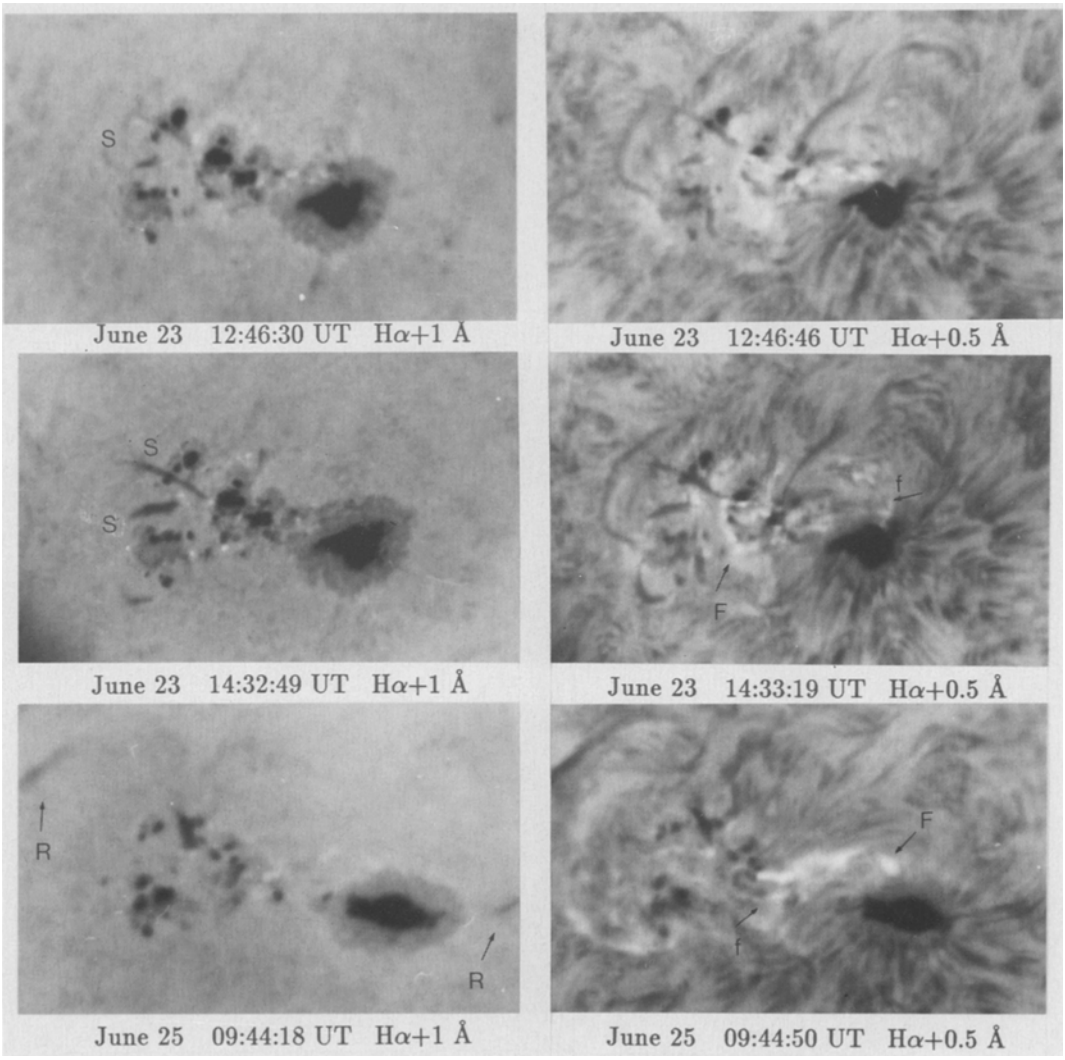

Fig. 5. Hα observations on 23 and 25 June, 1989 (Debrecen) showing the brightest kernels of flares (F), the faint ones (f), surges (S), and filament activities (R).

6. Separatrix Positions Compared with Flare Kernels and Current Cells

6.1. METHOD

Following the idea that flares are due to reconnection of magnetic field lines we model the vertical component of the observed magnetic field using magnetic charges in order to compute the separatrices. This method was first applied to observed data by Gorbachev and Somov (1988), and developed by Mandrini *et al.* (1991, 1993) and Démoulin *et al.* (1993).

After transformation to the solar local coordinates (horizontal and vertical),

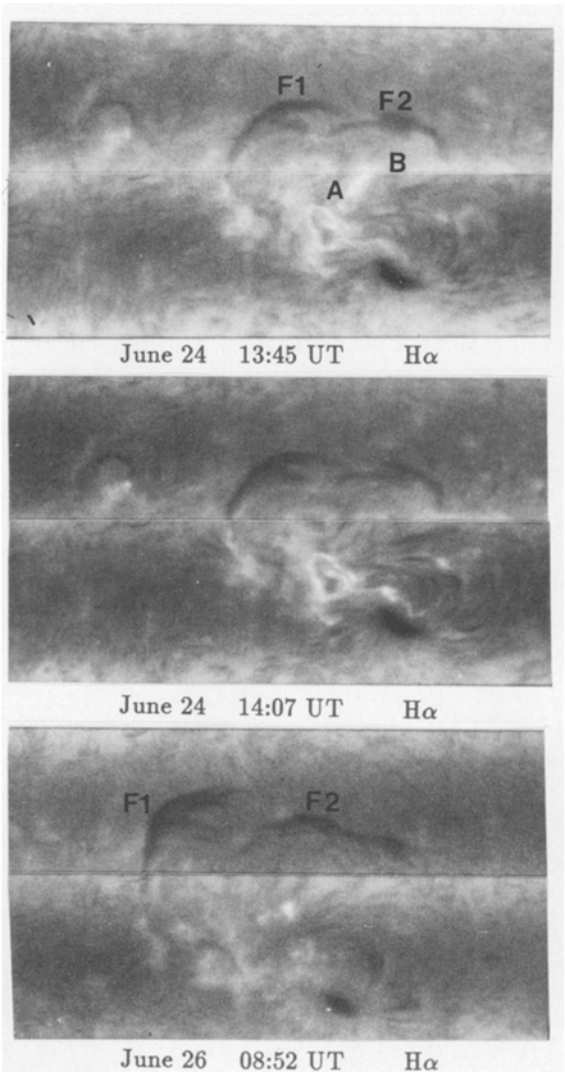

Fig. 6. Hα (MSDP, Meudon Observatory) observations on 24 and 26 June. Flare kernels (circular shape and straight one to the north–east of the leader spot), filaments F1, F2 and ejection of hot material (AB) are visible.

the observed magnetogram is modeled by a distribution of magnetic charges located below the photosphere. Because there are significant currents present in the observed region, we use a linear force-free field extrapolation, which is the only available magnetic field extrapolation for which separatrices can be obtained at present. If $\mathbf{B}_i(\mathbf{r} - \mathbf{r}_i)$ is the magnetic linear force-free field created at the position $\mathbf{r}$ by a magnetic charge i (located at $\mathbf{r}_i$ and with a unity charge value, see Démoulin and Priest (1992) for the expression $\mathbf{B}_i(\mathbf{r} - \mathbf{r}_i)$), the total magnetic field of N charges of intensity q_i is given by

$$\mathbf{B}(\mathbf{r}) = \sum_{i=1}^{N} q_i \mathbf{B}_i(\mathbf{r} - \mathbf{r}_i) \, .$$

A charge is positioned at the centre of each area with a strong field, and the charge intensity and depth are determined by a least-square fit between the above-mentioned model and the observed vertical magnetic field (see Démoulin *et al.*, 1993, for further details). In order to determine the best value of α the computed azimuth of the transverse magnetic field is compared to the observed one, and to the Hα fibrils.

Separatrices are computed by integrating field lines in both directions until a charge is reached (Démoulin, Hénoux, and Mandrini, 1992). To simplify the pattern of the separatrices, the charges are grouped, which means that all field lines ending (at both extremities) at any pair of charges in the group numbered i and j have the same connectivity (called $i - j$). The implication of this grouping is that we neglect separatrices between charges of the same group, assuming they belong to the same flux tube below the photosphere (we suppose that their relative motions are negligible, see Mandrini *et al.*, 1991). The magnetic field map is first modeled by a series of charges, and the computations are performed both in a potential configuration and in a linear force-free field configuration.

6.2. 23 JUNE, 1989

The negative polarity groups can be easily defined (Figures 8(a) and 8(b)). There is however no clear separation between the following positive polarities on the magnetograms and we need to use the proper motion of the spots and their evolution to divide them into groups, with reasonable confidence (Table V). We introduce only three positive groups in the separatrix computations $2 + 6$ (called 2), $2'$, and 4. In fact, as we show below, only the division between groups $2 + 2' + 6$ and 4 is important for understanding the flare ribbon positions. Dividing into more groups only adds more separatrices.

The azimuth of the transverse fields (Figures 9(a) and 9(b)) is then compared with the observed transverse field (Figure 3(a)). A value of $\alpha \approx 0.02\,\mathrm{Mm}^{-1}$ is found to give the best average fit to the data. The intersections of the separatrices with the chromosphere are compared with the positions of the flare kernels observed on 23 June at 14:33 UT (Figures 8(a) and 8(b)). The negative group 5 (*S4*) is exclusively connected with the south–east part of the following spots, and it is therefore surrounded by a separatrix which has no intersection with any other. In this simple (arcade like) geometry without a separator, no reconnection is thought to appear, in agreement with the observations, since no flares are reported there (only chromospheric activity is present to the south of group 5, which may be linked to an unresolved magnetic structure).

On the other hand, the group 3 (*S2*) is surrounded by a separatrix which intercepts others, and a small separator is present in its western part. One bright kernel (which may consist of two) is definitely situated along this separatrix. The two

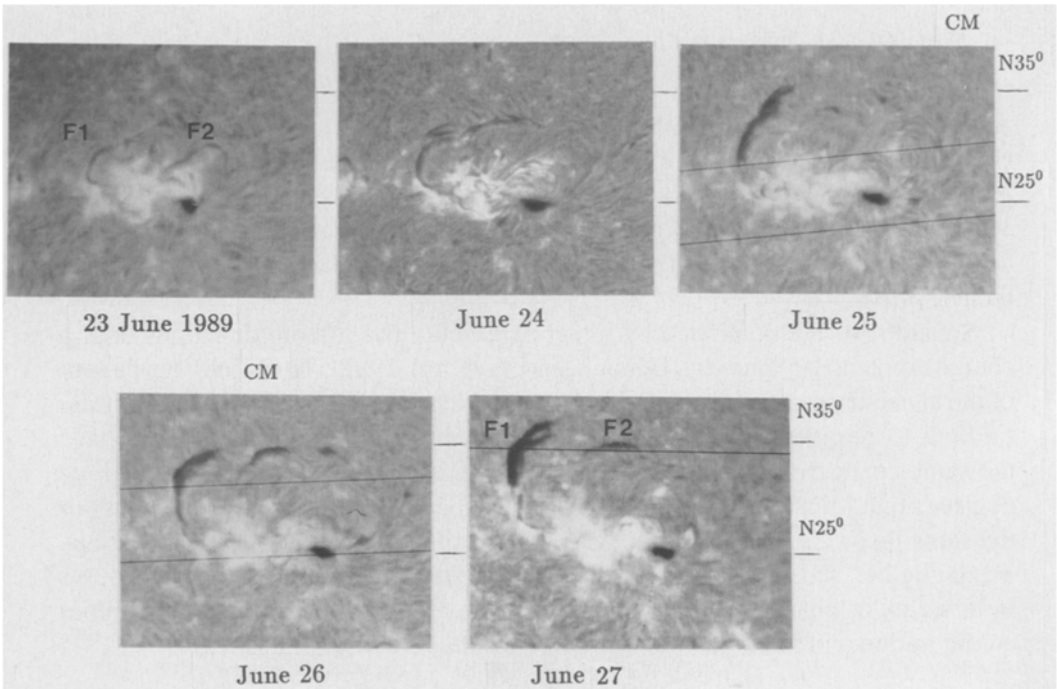

Fig. 7. Development and motion of filaments around AR 5555 between 23 and 27 June, 1989 (Meudon spectroheliograms). Positions of heliographic latitudes N25° and N35° are indicated for reference. Black lines in the pictures originate from dust on the slit of the spectroheliograph.

above-mentioned separatrices are present irrespective of the grouping used for the following polarity, and they are relatively insensitive to the presence of currents (compare Figure 8(a) to Figure 8(b)); therefore, these two separatrices are intrinsic properties of the active region.

The other separatrices are more sensitive to the adopted grouping. The separatrix associated to group 4 gives a better fit to the flare ribbons when a linear force-free field is used for the calculations than when a potential field is used. The remaining difference is attributed to the difference in the spatial repartition of currents between the linear force-free field (where current density is distributed like the magnetic field) and the nonlinear force-free field associated with the observed concentrated currents. The other bigger separatrix is needed to interpret the position of a small flare kernel to the north–east of group 4. The small kernel may be due to induced reconnection at the second separator by the global magnetic field evolution.

The magnetic field lines (Figures 9(c) and 9(d)) indicate approximately the connection between the photospheric current cells (see Section 4.3). The current cells 1 and 3 are at the border of the separatrices and of the flare kernels (Figures 8(a) and 8(b)) and in this case the energy of the flare is sorted in a twisted magnetic rope connecting the main polarities (and not in the minor bipole (3, 4) with reversed

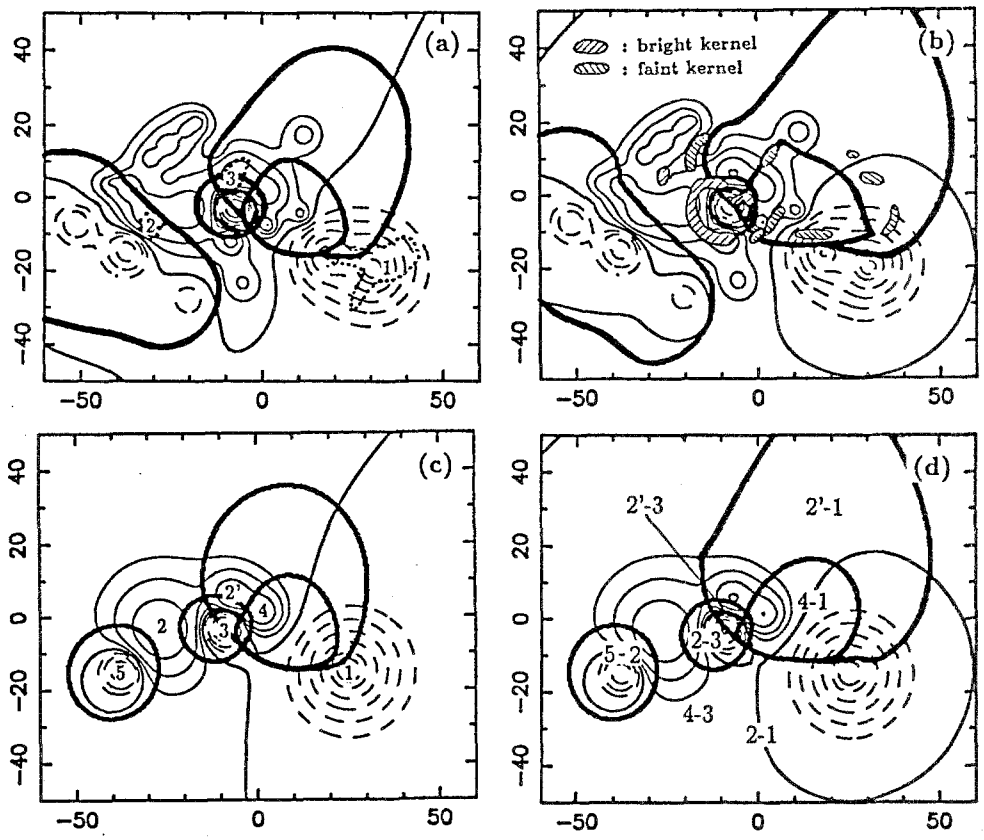

Fig. 8. Intersection (dark heavy lines) of the computed separatrices with the chomosphere over the active region on 23 June, 1989. The vertical magnetic field, B_z, is represented by the same isocontours as in Figure 3. (a) and (b) (respectively (c) and (d)) show a model with 25 (respectively 6) magnetic charges. Both a potential ((a) and (c)) and a linear ((b) and (d)) force-free field with $\alpha = 0.02$ Mm^{-1} are shown. In (a) the principal current cells (1, 2, 3) are superposed using dotted lines and in (b) hatched regions locate Hα flare kernels observed on 23 June at 14:33 UT. The position and group numbers of the magnetic charges used (respectively the magnetic connectivity) are given in (c) (respectively (d)).

orientation as found by Mandrini *et al.* (1991, 1993) for another region). This energy can be stored in a stable way until the reversed bipole (containing a small amount of energy) gives rise to a topological configuration (the presence of a separator) favourable for energy release (see Priest, 1991).

It is worth modeling the magnetic field configuration in the simplest possible way. A minimum of six charges is needed to describe all the separatrices (Figures 8(c) and 8(d)). The interacting separatrices are only slightly different from the previous model with 25 charges. This shows that only the large-scale structure of the magnetic field is relevant when the isolated polarities (which can have a small size) are properly taken into account. In the present active region the magnetic

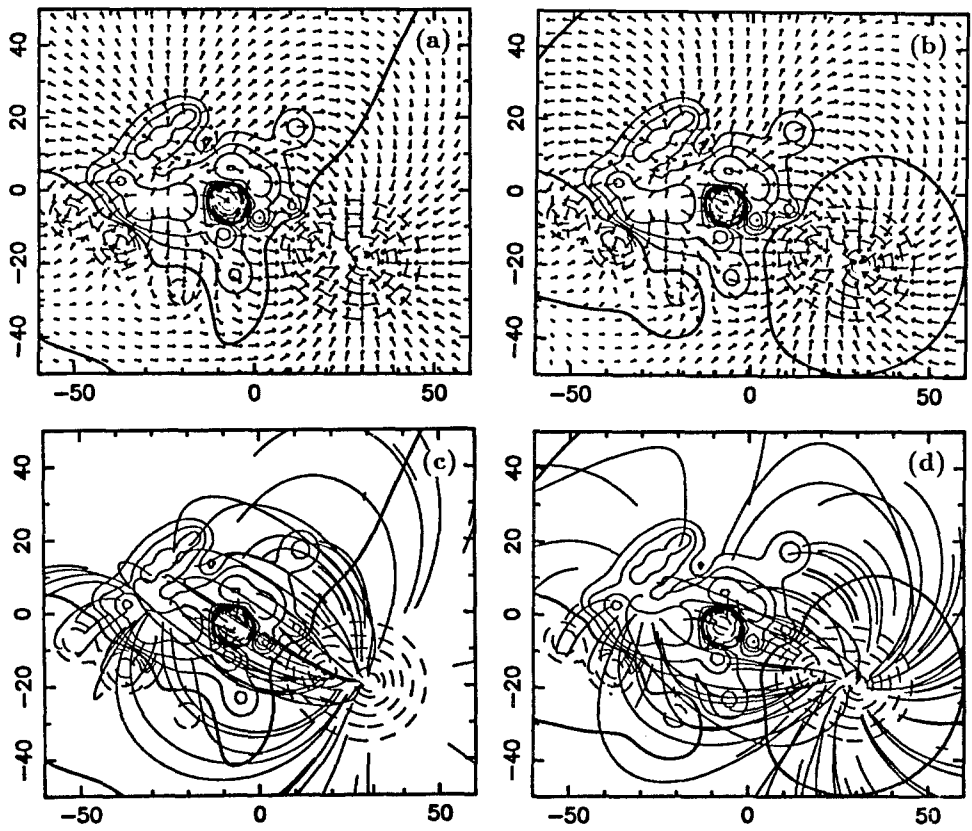

Fig. 9. Horizontal magnetic field computation ((a) and (b)) and magnetic field lines ((c) and (d)) with, respectively, a potential field assumption ($\alpha = 0$) for (a) and (c) or with a linear force-free field ($\alpha = 0.02$ Mm^{-1}) for (b) and (d). The magnetic field is modeled by 25 charges as in Figures 8(a) and 8(b).

configuration responsible for the flares can be modeled by only 4 charges: the main bipole (1, 2) and the reversed bipole (3, 4).

6.3. 25 JUNE, 1989

Like on 23 June, we group the magnetic polarities to emphasize the basic topology of the region (Table II). On 25 June spot *S2* has nearly moved out of the area occupied by f-polarity spots; only a 'tongue' of p-polarity is intruding into the f-polarity (Figure 4(b)). Spot *N14* is separated from other concentrations of the same polarity. Then spots *S2* and *N14* formed a well-separated bipole (3, 4). New spots appeared south of the following part of the active region (*S5, N11*) in the vicinity of the spots *S4, N5, N6*. They can be handled together in the groups (5, 6). At least four bipoles are interacting on 25 June (Table II): the main one (1, 2), the reversed bipole (3, 4), and two others (5, 6) and (7, 8). The interaction of these

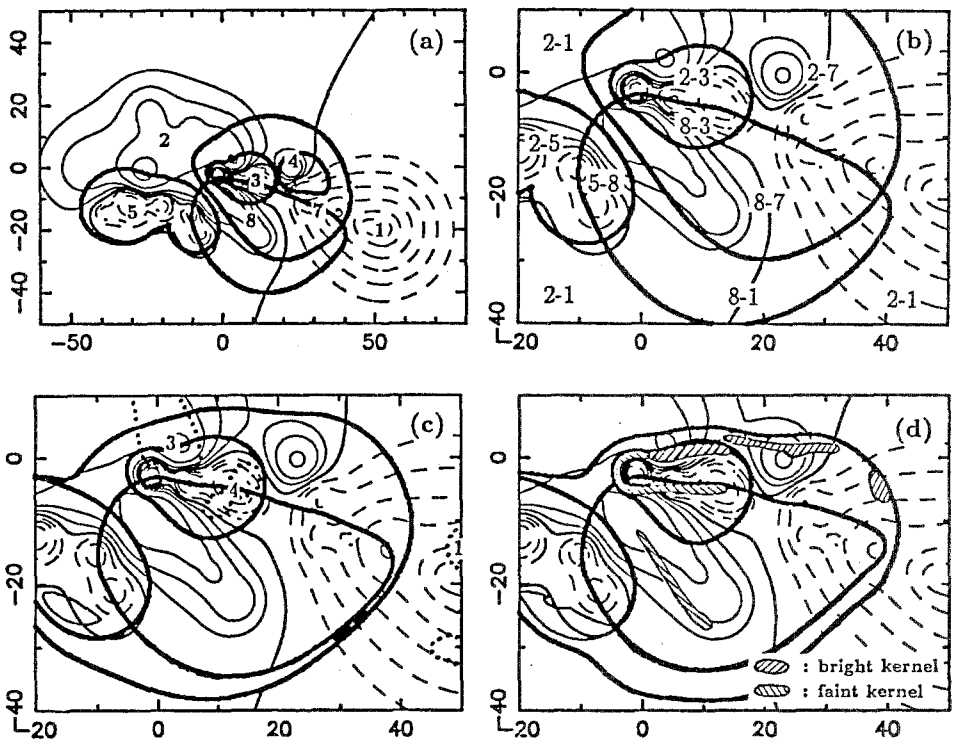

Fig. 10. Same as Figure 8 for the active region on 25 June. Twenty-eight charges are used in the model. (a) is a general view with the charge grouping given in Table II; (b)–(d) are enlargements by a factor 2 of the central part of (a) and the separatrices surrounding groups 4 and 6 are omitted. (a) and (b) (respectively (c) and (d)) are computed with a potential (respectively linear force-free) field with $\alpha = 0.00$ (respectively 0.01, 0.02) Mm^{-1}. In (b) the magnetic connectivity is indicated. Current cells 1, 3, and 4 (respectively Hα kernels) observed on 25 June are superposed in (c) (respectively (d)).

four bipoles makes the field topology complex, even if we use a potential field approximation (Figure 10(a)). A tentative scenario to understand the 25 June flare at 09:44 UT (see Figure 5) is given below.

First, let us analyse the eastern part of the active region. Compared to 23 June, the flux of the bipole (5, 6) has increased and a new polarity (group 8) is present to the west of it. This implies that the separatrix surrounding group 5 has grown and intersects the separatrix surrounding group 8 (Figure 10(a)). During the flare, reconnection at this new separator is then likely to produce the faint Hα brightenings seen to the south–east of the active region (Figure 5). The energy can be stored in field-aligned currents starting from current cell 2 (Figure 4(c)), but no counterpart (negative current) is observed in the opposite magnetic polarity close to the same separatrix. In any case, the main flare kernels are not related to this interaction.

Let us now analyse the separatrix complex around group 3 (spot *S2*. Judging from the position of the Hα flare ribbons (Figure 10(d)) group 3 is likely to play a key role in the eruption. Can the flare be the result of the interaction of bipole

(3, 4) with its surroundings as on 23 June? Separatrices are both present around groups 3 and 4 (Figure 10(a)). Increasing α from 0 to 0.02 Mm^{-1} inflates mainly the separatrix around 4 in the northwest, but is still does not intersect the separatrix surrounding group 3. Moreover, no Hα kernels can be related to this separatrix for any value of α. We conclude that group 4 is not important in the flaring process and therefore we include it in group 2 to simplify Figures 10(b–d).

Finally, let us focus on the most important separatrices. As shown in Figures 10(b–d), a complex pattern of three intersecting separatrices is needed to describe the position of the Hα kernels. The separatrix surrounding group 3 can be defined without ambiguity and is slightly distorted by an increase of α. It explains the U-shape of the faint eastern kernel and of one bright kernel. The separatrix surrounding group 8 intersects all other separatrices. It is slightly deformed by increasing α, it can explain the position of one faint kernel but it cannot explain the brightest flare kernels. The separatrix surrounding group 7 is very sensitive to the value of α (compare Figures 10(b–d)). With $\alpha = 0$, its south–eastern part may explain the faint kernel located above group 8, while with $\alpha \approx 0.02$ Mm^{-1} (determined from the transverse field magnetogram), its northern part gives a reasonably good position of the brightest kernels. Thus the distortion of the magnetic field by field-aligned currents is a clue in understanding the position of the brightest kernels. However, since some separatrices are very sensitive to the field-aligned current distribution, the linear force-free field model used here gives only a first approximation.

Our proper-motion measurements show that spot *S2* (group 3) moves towards the big preceding spot, while all spots around it are moving in the opposite direction, towards the E–NE. These shearing motions are able to create coronal currents, then to store magnetic energy. This free energy can be released when the currents reach the separatrices. The locations of the flare observed on 23, 24, and 25 June support this scenario. When spot *S2* (group 3) approaches the leading spot and fades on 26 June the flare activity in this region disappears as well.

The observed currents are mainly located in the main bipole (current cells 1 and 3 in Figure 10(c)) but unlike 23 June, current cell 1 is not at the border of a separatrix (Figure 10(c)). On 25 June, the energy may be stored in field-aligned current going from current cell 3 to 4, but present data have insufficient spatial resolution to prove this statement (group 4 is small and nearly surrounded by the opposite polarity, its measured magnetic field is mixed with the opposite polarity).

The flare of 25 June is complex in the sense that at least 7 magnetic groups are present and the field is far from being potential. However, the topological model developed initially for a simpler configuration (Gorbachev and Somov, 1988) can be applied successfully to interpret the observations. The flare of 25 June is the result of an interaction of the main bipole (groups 1 and 2) with other polarities (mainly groups 3, 7, and 8).

7. Conclusions

The sunspot group in AR 5555 has a basically bipolar character (*S1* and the following polarity spots) but it is perturbed by the presence of three other bipoles making the magnetic configuration suitable for flare activity. One bipole (*S2–N14*) is located in the centre of the active region with a direction opposite to that of the main bipole, another bipole is situated at the southern edge of the following polarity *S4, S5, N5, N6, N11* and the last bipole appears in the middle part of the group, but with an orientation nearly parallel to the main one (*N9–S3*).

The strongest shearing motions in the AR appear between the main and the minor reversed bipole in the centre of the AR. There opposite polarity spots move in different directions, with peak relative velocity (between 23 and 24 June) of 0.17 km s^{-1}. Between 23 and 25 June the p spot *S2* gradually separates from the following (north) polarity and moves closer to the principal preceding (south) polarity spot *S1*. Flare activity, which is intense in the vicinity of *S2* when it is an isolated S pole in a N polarity environment, ceases when its isolation is over.

Magnetic field extrapolations, using observed (Potsdam) photospheric vertical magnetic fields, are made with both potential and linear force-free field assumptions. The value of the twist in the latter case is deduced from the direction of the observed transverse magnetic field. The topology of such fields is investigated using a method developed by Mandrini *et al.* (1991). We find that the Hα flare ribbons are located near the intersection of the separatrices with the chromosphere and that linear force-free field approximation gives better results than the potential approximation. We interpret the small discrepancy between the observed and modeled locations as the result of a deviation of the magnetic field configuration from a linear force-free field, as the observed currents are more concentrated than the linear force-free field implies.

With this model we attribute flares to magnetic interactions between 2 or 3 bipoles, the energy being stored in field-aligned currents. It is worth noting that flaring occurs only when the magnetic configuration has intersecting separatrices; an isolated magnetic polarity or the presence of important currents not being a sufficient condition for flaring.

Acknowledgements

We would like to thank Á. Kovács for providing us with the photospheric and chromospheric observations obtained at Debrecen, R. Hellier and C. Coutard for the spectroheliograph and MSDP observations at Meudon. We are grateful to Dr W. van Driel for a critical reading of the paper. One of us (L.v.D.-G.) was supported by Observatoire de Paris during her visits there. We thank the unknown referee with a good sense of humour for his/her thorough reading and helpful suggestions which greatly helped to improve the paper.

References

Abramenko, V. I., Gopasyuk, S. I., and Ogir, M. B.: 1991, *Solar Phys.* **134**, 287.
Canfield, R. C., de La Beaujardière, J. F., and Leka, D. D.: 1991, *Phil. Trans. Roy. Soc. London* **A336**, 381.
Démoulin, P. and Priest, E. R.: 1992, *Astron. Astrophys.* **258**, 535.
Démoulin, P., Hénoux, J. C., and Mandrini, C. H.: 1992, *Solar Phys.* **139**, 105.
Démoulin, P., Priest, E. R., and Ferreira, J.: 1991, *Astron. Astrophys.* **245**, 289.
Démoulin, P., van Driel-Gesztelyi, L., Schmieder, B., Hénoux, J. C., Csepura, G., and Hagyard, M. J.: 1993, *Astron. Astrophys.* **271**, 292.
Dezsö, L., Gerlei, O., and Kovács, Á.: 1988, 'Debrecen Photoheliographic Results', *Publ. Debrecen Obs. Heliographic Series*, No. 1, p. 11.
Ding, Y. J., Hagyard, M. J., de Loach, A. C., Hong, Q. F., and Liu, X. P.: 1987, *Solar Phys.* **109**, 307.
Gaizauskas, V.: 1989, *Solar Phys.* **121**, 135.
Gorbachev, V. S. and Somov, B. V.: 1987, *Solar Phys.* **109**, 81.
Hagyard, M. J.: 1988, *Solar Phys.* **115**, 107.
Hénoux, J. C. and Somov, B. V.: 1987, *Astron. Astrophys.* **185**, 305.
Hofmann, A. and Kálmán, B.: 1991, *Astron. Astrophys.* **241**, 203.
Hofmann, A., Ruždjak, V., and Vršnak, B.: 1989, *Hvar Obs. Bull.* **13**, No. 11.
Lin, Y. and Gaizauskas, V.: 1988, *Solar Phys.* **115**, 107.
Mandrini, C. H., Démoulin, P., Hénoux, J. C., and Machado, M. E.: 1991, *Astron. Astrophys.* **250**, 541.
Mandrini, C. H., Rovira, M. G., Démoulin, P., Hénoux, J. C., Machado, M. E., and Wilkinson, L.: 1993, *Astron. Astrophys.* **272**, 609.
Mein, P.: 1977, *Solar Phys.* **54**, 45.
Newton, H. W. and Nunn, M. L.: 1951, *Monthly Notices Roy. Astron. Soc.* **111**, 413.
Priest, E. R.: 1991, *Phil. Trans. Roy. Soc. London* **A336**, 363.
Romanov, V. A. and Tsap, T. T.: 1990, *Soviet Astron.* **34**, 656.
Schmieder, B., van Driel-Gesztelyi, L., Hénoux, J. C., and Simnett, G. M.: 1991, *Astron. Astrophys.* **244**, 533.
Somov, B. V.: 1986, *Adv. Space Res.* **6**(6), 177.
Staude, J.: 1970a, *Solar Phys.* **12**, 84.
Staude, J.: 1970b, *Solar Phys.* **15**, 102.
Vekstein, G. E., Priest, E. R., and Amari, T.: 1991, *Astron. Astrophys.* **243**, 492.
Wilkinson, L. K., Emslie, A. G., and Gary, G. A.: 1992, *Astrophys. J.* **392**, L39.